The influence of convective aggregation on the stable isotopic composition of water vapor: Implications for the humidity of the troposphere

Joseph Galewsky[1], Matthias Schneider[2], Christopher Diekmann[2,3], Addisu Gezahegn[4,5], Sandrine Bony[5], Camille Risi[5], Kerry Emanuel[6], Helene Brogniez[7]

[1]Department of Earth and Planetary Sciences, University of New Mexico, Albuquerque, New Mexico
[2]Institute of Meteorology and Climate Research (IMK-ASF), Karlsruhe Institute of Technology, Karlsruhe, Germany
[3]Now at: Software Solutions Department, Telespazio Germany GmbH, Darmstadt, Germany
[4]Computational Data Science Program, Addis Ababa University, Addis Ababa, Ethiopia
[5]LMD/IPSL, Sorbonne University, CNRS, Paris, France
[6]Lorenz Center, Massachusetts Institute of Technology, Cambridge, Massachusetts
[7]Laboratoire Atmosphères, Milieux, Observations Spatiales (LATMOS/IPSL, UVSQ Université Paris-Saclay, Sorbonne Université, CNRS), Guyancourt, France

Key Points:

- Remote sensing datasets are used to study the impact of convective aggregation on the atmospheric hydrologic cycle in the global tropics.
- Unaggregated convection is associated with top-heavy vertical velocity profiles, increased mixing ratios, and decreased water vapor isotopic ratios.
- Aggregated convection is associated with bottom-heavy vertical velocity profiles and a positive correlation between mixing ratio and water vapor isotopic ratios.

Corresponding author: Joseph Galewsky, galewsky@unm.edu

Abstract

Remote sensing datasets of water vapor isotopic composition are used along with objective measures of convective aggregation to better understand the impact of convective aggregation on the atmospheric hydrologic cycle in the global tropics (30°N to 30°S) for the period 2015-2020. When convection is unaggregated, vertical velocity profiles are top-heavy, mixing ratios increase and water vapor δD decreases as the mean precipitation rate increases, consistent with partial hydrometeor evaporation below anvils into a relatively humid atmospheric column. Aggregated convection is associated with bottom-heavy vertical velocity profiles and a positive correlation between mixing ratio and δD, a result that is consistent with isotopic enrichment from detrainment of shallow convection near the observation level. Intermediate degrees of aggregation do not display significant variation in δD with mixing ratio or precipitation rate. Convective aggregation provides a useful paradigm for understanding the relationships between mixing ratio and isotopic composition across a range of convective settings. The results presented here may have utility for a variety of applications including the interpretation of paleoclimate archives and the evaluation of numerical simulations of convection.

Plain Language Summary

Convective clouds in the atmosphere can aggregate in a variety of ways, from individual cells to larger systems like tropical cyclones and squall lines. Some recent studies have examined how the aggregation of clouds affects water vapor, which can have an impact on the Earth's climate. In this study, we use remote sensing measurements of water vapor isotopic composition along with objective measurements of cloud organization to understand how the convective aggregation affects the water cycle in the tropics from 2015 to 2020. When clouds are not aggregated, there is more moisture in the atmosphere and water vapor becomes more isotopically depleted with increasing rain rates, while aggregated clouds are associated with less moisture and isotopic enrichment of water vapor with increasing rain rates. These findings could be useful for understanding past climates and for evaluating computer simulations of clouds and climate.

1 Introduction

Convective clouds exhibit a wide range of organizational styles, from randomly scattered convective cells to mesoscale convective systems and tropical cyclones (Holloway

et al., 2017). Numerical modeling studies with increasingly high resolution have yielded important insights into the processes that govern the organization or aggregation of convective clouds (Held et al., 1993; Bretherton et al., 2005; Muller & Held, 2012), and have shown that aggregation is favored by a combination of surface flux, moisture, and radiative feedbacks (Wing et al., 2017). Several recent studies have explored how the insights from modeling studies may be applied to understanding the influence of convective aggregation on the climate of the tropics (Bony et al., 2020; Semie & Bony, 2020) and how convective aggregation influences humidity (Wing et al., 2017; Tobin et al., 2012). In particular, unaggregated convection is often associated with a moister atmosphere, a large extent of upper-tropospheric clouds, and a top-heavy ascent profile, while aggregated convection is more commonly associated with a drier atmosphere, little upper-tropospheric cloud cover, and a bottom-heavy ascent profile (Tsai & Mapes, 2022). Such variations in humidity have impacts on outgoing longwave radiation, with important implications for climate (Bony et al., 2020).

While modeling studies provide important clues about the influence of convective aggregation on humidity, extending these insights to observations can be more challenging owing to the difficulty of diagnosing the range of processes that control humidity. The stable isotopic composition of atmospheric water vapor is a sensitive recorder of phase changes of water substance and mixing between different airmasses (Galewsky et al., 2016; Noone, 2012; Craig, 1961). The isotopic composition of water vapor in an air parcel reflects its history of phase changes and mixing with other air parcels. Whenever there is a phase change, heavier isotopologues preferentially remain in the condensed phase. The evaporation of condensate can influence the stable isotopic composition of water vapor through the partial evaporation of isotopically light water from hydrometeors (Risi et al., 2021; Lawrence et al., 2004; Lee & Fung, 2008). Mixing between water vapor in different airmasses yields a resulting isotopic composition that is a humidity-weighted combination of the different airmasses that are mixed (Galewsky & Hurley, 2010). Diluting (mixing) a moist airmass with a much drier airmass has only a weak impact on the isotopic composition of the mixture (Risi et al., 2019). In such a case, the mixture will have a lower overall mixing ratio but the isotopic composition of the water vapor will overwhelmingly reflect the isotopic composition of the moister airmass owing to the much greater water vapor abundance in the moist airmass. Stable isotopic measurements may

thus provide a useful pathway for improved understanding of how convective aggregation influences humidity.

Lacour et al. (2018) explored the impact of the depth of convection and precipitation intensity on the isotopic composition of mid-tropospheric water vapor. They showed how shallow convection can isotopically enrich the middle troposphere through the convective detrainment of boundary layer air; in contrast, deep convection can isotopically deplete the middle troposphere through partial hydrometeor evaporation into relatively humid air as the lighter isotopologues preferentially evaporate, and downdrafts of isotopically depleted water vapor. In the former case, latent heating is observed to peak in the lower atmosphere, while latent heating peaks in the upper troposphere for deeper convection. In general, the mixing ratio (q) is correlated with water vapor δ values, meaning that more humid air parcels tend to be more isotopically enriched. This positive correlation can be attributed to mixing of isotopically-enriched boundary layer air into the free troposphere by convection. In cases of top-heavy large-scale ascent, however, q and δ are anti-correlated. Lacour et al. (2018) found that anti-correlated $q-\delta$ pairs are associated with deep convection and hydrometeor evaporation from above, although they also suggested that convective downdrafts could play a role in this anti-correlation. Torri et al. (2017) showed that different structures of vertical velocities are associated with different isotopic abundances and that precipitation in the eastern part of the Pacific is more enriched than in the western part, implying that velocity profiles in the East are more bottom heavy than in the West Pacific. Similar results were found by Diekmann, Schneider, Knippertz, et al. (2021), who found that different combinations of air mass mixing, Rayleigh condensation during convection, and microphysical processes that deplete the vapor determine the final isotopic composition in the Sahelian troposphere during the monsoon. While these studies did not explicitly focus on convective aggregation, their results, along with previous studies that have indicated systematic links between aggregation and humidity, suggest that there should be a coherent link between convective aggregation and the isotopic composition of water vapor. This is the hypothesis we test here.

This study is facilitated by two key recent advances. First is our ability to quantitatively measure the state of convective aggregation from observations. A quantitative metric for the degree of aggregation is essential for a thorough analysis, and several approaches have been developed in recent years. Tobin et al. (2012) developed a Simple

Convective Aggregation Index (SCAI) based on the numbers of convective clusters within a region along with the average distances between clusters. Tompkins and Semie (2017) developed the I_{org} index for use in numerical models, based on statistical comparisons with a pure random process. This method was extended to observations by Semie and Bony (2020) who used minima in infrared brightness temperatures to identify convective clusters. We use the I_{org} metric in this study, although similar results are obtained using SCAI or the number of convective clusters in a domain. The other key advance is the global, multi-year MUSICA IASI dataset of paired H_2O and δD (Diekmann, Schneider, Ertl, et al., 2021). This dataset provides twice-daily global observations, giving us an unprecedented window into the global isotopic composition of atmospheric water vapor. In this study, we take advantage of these advances to disentangle the links between convective aggregation, humidity, and the stable isotopic composition of water vapor.

2 Methods and Datasets

We report the isotopic composition of water vapor in permil (‰), relative to Vienna Standard Mean Ocean Water (VSMOW) using δ notation (e.g. $\delta D = (R/R_{VSMOW} - 1) \times 1000$, where R is the D/H ratio). The principal dataset used in this study is the global, multi-year MUSICA IASI H_2O and δD dataset (Diekmann, Schneider, Ertl, et al., 2021), which is based on radiance measurements from the nadir thermal infrared sensor IASI on board the Metop satellites of EUMETSAT. The satellite ground pixel diameter is 12 km (at nadir), with a full swath width of 2200 km We analyze the complete dataset from 2015 through 2020 and follow the diagnostic critera recommended by Diekmann, Schneider, Ertl, et al. (2021). We select only those data points with no or little contamination from clouds, fair or good retrieval fit quality, good vertical sensitivity, and with δD error less than 40‰ for a total of over 42 million paired H_2O and δD retrievals from the $30°S$ to $30°N$ latitude band. Except for very dry conditions, the errors are within 25‰. The focus of the dataset is on mid-tropospheric abundances of H2O and δD, with the main sensitivity limited to the 2-7 km range. We focus on retrievals centered at 710 hPa, which samples from 870 hPa to 500 hPa (Diekmann, Schneider, Ertl, et al., 2021).

In an idealized picture of condensation, water vapor in the atmosphere undergoes Rayleigh distillation, during which water vapor in an ascending air parcel condenses and fractionates such that heavier isotopologues of water preferentially move into the condensate, leaving the remaining vapor depleted in the heavier isotopologues. This pro-

cess leads to a change in the isotopic composition of both the precipitation that forms and the remaining water vapor as heavier isotopologues preferentially fractionate into the condensed phase. As a result, Rayleigh distillation is a useful starting point for understanding how to use isotopic measurements to trace the movement of water through the hydrologic cycle. As described in previous studies (Galewsky, 2018a, 2018b) the difference, in permil, between an isotopic measurement at a given mixing ratio and the δ-value of the idealized Rayleigh distillation process to the same mixing ratio is a useful metric that can be interpreted in terms of moistening and mixing processes. This quantity will be referred to here as D_{rl}. This metric is similar to the δD_q used by Bailey et al. (2017). A high, or more positive, value of D_{rl} occurs when an isotopic value lies above a Rayleigh curve and is interpreted as representing a small degree of moistening of a dry, isotopically-depleted airmass by a moist, isotopically-enriched airmass (Galewsky & Hurley, 2010), while low or negative of D_{rl} are interpreted as representing greater evaporative moistening. This latter process is sometimes referred to as "super-Rayleigh" (Noone, 2012). For this study, we computed the relevant parameters for Rayleigh distillation from averaged ERA reanalysis between 30°N and 30°S from the 2015-2020 period. The starting isotopic composition was computed using the closure assumption of Merlivat and Jouzel (1979). With an average SST over the tropical domain of 299.5 K, 2 meter air temperature of 298.1K, 2m RH of 77.5%, we calculated a starting water vapor δD of $-72.6‰$ and a lifted condensation level of 940 hPa.

We characterize the spatial organization of convective clusters using the I_{org} index of Tompkins and Semie (2017) and Semie and Bony (2020), which is computed using 3-hourly inter-calibrated infrared brightness temperature (T_b) from GridSat-B1 (Knapp et al., 2011) between 30°N and 30°S every 1° in a moving 10°×10° box, for a total of 14,400 domains within the tropics. For each 3-hourly snapshot of T_b, we identify deep convective centroids as the points of local minima in the T_b field. Once the convective centroids are identified, the distances between nearest-neighbor (NN) centroids are calculated. The I_{org} index compares the cumulative density function of the calculated NN distances (NNCDF) with that expected from a random distribution of the same number of convective centroids. For a random distribution associated with a Poisson process, the cumulative density function (PNNCDF) is given by a Weibull function as:

$$PNNCDF = 1 - \exp(-\lambda \pi r^2) \tag{1}$$

where λ is the number of convective centroids per unit area and r is the nearest-neighbor distance. Values of I_{org} that are larger than 0.5 correspond to a clustered distribution of deep convective clouds, while $I_{org} = 0.5$ represents randomly distributed convection. Further details on this method are provided in Tompkins and Semie (2017) and Semie and Bony (2020). The 3-hourly I_{org} data is interpolated in time and space to each MUSICA IASI retrieval.

Precipitation data are derived from the GPM IMERG Final Precipitation L3 1 day $0.1^\circ \times 0.1^\circ$ V06 ($GPM-3IMERGDF$) dataset (Huffman et al., 2019). Latent heating profiles are from the GPM DPR Spectral Latent Heating Profiles L2 1.5 hours 5 km V07 product (Team, 2022). Cloud-top pressure and high-cloud fraction data is from MODIS (Platnick et al., 2003-02). These datasets are interpolated to the time and location of the MUSICA IASI retrievals.

Relative humidity (RH) profiles are derived from the SAPHIR sounder on the Megha-Tropiques satellite (Brogniez et al., 2016; Sivira et al., 2015). The satellite samples a given point between 3 and 5 times daily, and here we use daily averages of the operational Level 2 RH product gridded at a $1^\circ \times 1^\circ$ resolution, in which we retain data with at least 95% valid RH values within each gridbox. The SAPHIR RH data is useful as an independent measure of humidity because the retrieval does not rely on a priori assumptions about temperature profiles or integrated water vapor content.

3 Results

3.1 Global maps sorted by degree of aggregation only

We begin by investigating the global geographic relationships between I_{org}, mixing ratio, and δD. In Figures 1 and 2, we bin-average all of the 2015-2020 data into $1^\circ \times 1^\circ$ domains. For Figs. 1A and 2A, we show the number of data points corresponding to $0.5 < I_{org} < 0.65$, and $I_{org} > 0.8$, respectively, while for Figures 1B-D we show average values of mixing ratio, δD, and D_{rl} for all precipitation rates. In Fig. 2B-D, we show the differences between the high I_{org} and low I_{org} fields. Unaggregated convection ($I_{org} < 0.65$) most frequently occurs over the Maritime Continent, the western Pacific Ocean, and the eastern Indian Ocean (Fig. 1A), with additional clusters over tropical Central and South America and, to a lesser extent, over Central Africa. The 710 hPa mixing ratios are generally higher (in excess of 7 g/kg) in regions of frequent unaggregated con-

vection, especially over the Maritime Continent, South America, Africa, and South Asia (Fig. 1B). Water vapor δD (Fig. 1C) over these regions is generally around -200‰, with a particularly striking exception over Africa, where δD values are generally above -150‰. Sharply negative values of D_{rl} (Fig. 1D) are centered over the Maritime Continent, with values reaching below -100‰. Other prominent lows in this field are located over South America and in the tropical Pacific, reaching values near -80‰. The negative values of D_{rl} and relatively high mixing ratios are consistent with evaporative moistening associated with deep convection (Noone, 2012).

Highly-aggregated convection ($I_{org} > 0.8$) occurs less frequently overall than unaggregated convection (Fig. 2A), but there are regions of higher occurrence in the tropical Pacific and Atlantic Oceans, as well as the westernmost Indian Ocean, and, to a lesser extent, in the North Pacific basin. Regions of aggregated convection are drier than regions of unaggregated convection (Fig. 2B), with mixing ratios up to 3 g/kg lower, and more isotopically enriched, wth δD values up to 40‰ higher over the Maritime Continent, Africa, and South America. The D_{rl} fields are also higher everywhere for aggregated convection (Fig. 2D), with the differences reaching over 40‰ throughout the Tropics. Along with the lower mixing ratios for aggregated convection, these D_{rl} values suggest less evaporative moistening for aggregated convection than for unaggregated convection.

Precipitation rates are spatially variable and differ widely for weakly aggregated (Fig. 3A) and strongly aggregated (Fig. 3B) convection. Within the Intertropical Convergence Zone and over the Maritime Continent, average rainfall exceeds 12 mm/day for weakly aggregated convection, while precipitation rarely exceeds 4 mm/day for strongly aggregated convection. In line with previous studies (Tobin et al., 2012; Lacour et al., 2018), a fuller picture requires sorting the isotopic data by precipitation rate in order to to distinguish the impact of convective organization from the impact of convective intensity.

3.2 Sorting by degree of aggregation and precipitation rate

In Figure 4, we bin-average all of the MUSICA IASI isotopic and mixing ratio data by I_{org} and precipitation rates. The 710 hPa mixing ratios generally decrease with increasing I_{org} and decreasing precipitation rate, from around 8 g/kg for unaggregated con-

vection with high precipitation rates to below 4 g/kg for aggregated convection and low precipitation rates. In general, the mixing ratios increase with increasing precipitation rates, but aggregated convection is always associated with drier conditions than unaggregated convection, and the rate of moistening with precipitation rate is greater for low values of I_{org}. For I_{org} below 0.65, the water vapor δD decreases with increasing precipitation rates from around $-180‰$ at the lowest precipitation rates to around $-195‰$ at 20 mm/day. For I_{org} of around 0.75, δ values remain roughly constant at $-178‰$, even with increasing precipitation rates. At higher vaues of I_{org}, the δ values increase with increasing precipitation rates, rising from $-180‰$ to over $-170‰$ at 20 mm/day. D_{rl} is shown Fig. 4C and decreases sharply with precipitation rate for I_{org} below 0.6, from $-30‰$ at the lowest precipitation rates to nearly $-100‰$ at precipitation rates of 20 mm/day. For higher values of I_{org}, precipitation rates above around 2 mm/day do not significantly affect D_{rl}, but D_{rl} rises from around $-65‰$ for $I_{org} = 0.7$ to around $-25‰$ for $I_{org} > 0.95$. These results are consistent with moistening and isotopic depletion of water vapor for weakly aggregated convection and only modest moistening along with isotopic enrichment for more highly-aggregated convection.

A common and convenient way to visualize the co-variability of mixing ratio and isotopic composition is a $q-\delta$ plot, and we show three such figures in Figure 5, corresponding, respectively, to low, medium, and high values of I_{org}. In all cases, the mixing ratio increases with increasing precipitation rate (which is shown by the colored dots), but the slope of the $q-\delta$ relationship systematically varies with I_{org}. As initially illustrated in Figure 4, we can more clearly see the negative correlation between q and δD for low values of I_{org} in panel A, how δD is nearly invariant with increasing mixing ratio and precipitation rate for intermediate values of I_{org} in panel B, and the positive correlation between q and δD for high values of I_{org} in panel C. These relationships illustrate how the paradigm of convective aggregation allows us to efficiently discriminate positive and negative q-δD correlations that have been previously reported (Lacour et al., 2018; Diekmann, Schneider, Knippertz, et al., 2021).

3.3 Processes governing I_{org}-precipitation rate-δD relationships

Now that we have established that there is indeed a systematic relationship between convective aggregation and the isotopic composition of water vapor, we seek to understand the suite of processes that govern these relationships. Figure 6 shows profiles of

ERA vertical velocity (ω, in panel A) and SAPHIR relative humidity (B) averaged by I_{org}. The strongest ascent is associated with I_{org} below 0.6 and is centered at around 350 hPa. The strongest subsidence is associated with the highest values of I_{org} and is also centered at around 350 hPa. In between these extremes is a transition from ascent through most of the troposphere to subsidence through most of the troposphere. There is a reasonably close association between the vertical velocities shown in panel (A) and the RH shown in panel (B). The highest relative humidity, about 70% is found between 800 hPa and 900 hPa for I_{org} below 0.6, with a relatively sharp transition to lower RH at around 500 hPa. The lowest RH, below around 20% is associated with strong subsidence above 400 hPa and I_{org} above around 0.9. The deep layer of humid air at low I_{org} is consistent with the observed anti-correlation between moistening and isotopic composition. As shown by Lawrence et al. (2004) and Lee and Fung (2008), partial evaporation of condensate from deep convection in a relatively moist atmosphere can lead to an isotopic depletion with increasing precipitation rates.

The impact of precipitation rate on the top-heaviness of the vertical velocity profiles as a function of I_{org} is shown in Figure 7. The difference in ω between the 920 hPa and 300 hPa levels sharply increases with precipitation rate for the lowest values of I_{org}, representing an increase in top-heaviness with increasing precipitation rate, but this effect decreases with increasing values of I_{org}. Above I_{org} of around 0.75, the profiles become bottom-heavy, with increasing bottom-heaviness at higher values of I_{org} regardless of precipitation rate.

The dependence of convective depth and intensity on I_{org} are further illustrated in Figure 8. Figure 8A shows how the high cloud fraction decreases with increasing I_{org} from over 0.8 for low I_{org} to 0.2 for high values of I_{org}. Figure 8B shows that cloud top pressure decreases sharply with decreasing I_{org} and with increasing precipitation rates. Cloud top pressure increases from 350 hPa for weakly aggregated, strongly precipitating convection to 750 hPa for strongly aggregated, weakly precipitating convection. Finally, Figure 8C shows the sharp decrease in the altitude of maximum latent heating with increasing I_{org}, ranging from nearly 6 km for unaggregated convection to below 3 km for highly aggregated convection. From this data, it appears that the maximum in δD seen in Fig. 4 occurs for aggregated convection ($I_{org} > 0.8$) when the altitude of maximum latent heating rises above the IASI observation level of 710 hPa, suggesting that

the maximum δD in this dataset may be related to outflow of convection near the level of observation.

Figure 9 summarizes our interpretation of the relationships between aggregation and isotopic composition presented above. Unaggregated convection ($I_{org} < 0.6$) is associated with large high-cloud fractions, strong ascent, and a high altitude of maximum latent heating. Evaporation of hydrometeors below anvils acts to moisten the troposphere throughout a deep level while reducing the water vapor δD to values below a reference Rayleigh distillation curve, yielding D_{rl} values well below zero. At high values of I_{org} (above 0.8), water vapor δD reaches its maximum at rain rates above 5-10 mm/day as the altitude of maximum latent heating rises just above the main MUSICA IASI observation level of 710 hPa. We interpret this δD maximum as reflecting convective outflow of isotopically-enriched water vapor. Water vapor D_{rl} is less negative than for unaggregated convection, rising to just above $-20‰$ for $I_{org} > 0.9$ and low precipitation rates, suggesting a reduced influence of condensate evaporation along with mixing with dry, isotopically-depleted airmasses from aloft.

4 Discussion

Our results illustrate how convective aggregation exerts a significant impact on atmospheric water vapor. Water vapor associated with deep, unaggregated convection with top-heavy vertical velocity profiles is isotopically depleted relative to shallow, aggregated convection with bottom-heavy vertical velocity profiles at the same precipitation rate and the same observational level, likely owing to a greater degree of condensate evaporation in the unaggregated case. Because the volume of cloud-free air is typically much larger than the volume of cloudy air, satellites are mostly sampling cloud-free air and our results here are of course limited to those clear-sky settings in which satellite retrievals are possible. A valuable complement to the present study, which is focused exclusively on water vapor, would be to extend this analysis to precipitation data. Such a study would provide valuable insight into how these processes govern not just the environmental water vapor, but the full suite of condensation and precipitation processes in convection under a variety of aggregated conditions.

Several studies have found that organized convection in the form of squall lines (Risi et al., 2008; Tremoy et al., 2014), tropical cyclones (Lawrence et al., 2004; Chakraborty

et al., 2016; Xu et al., 2019) and mesoscale convective systems (Kurita, 2013) is associated with more depleted water vapor, results that appear to be at odds with the present study. This discrepancy is likely at least partially related to the complicated relationships between convective aggregation with vertical velocity profiles. As was shown here and by Tsai and Mapes (2022) and Tobin et al. (2012), unaggregated convection is, on average, associated with more top-heavy vertical velocity profiles than aggregated convection, but those averages hide the variability in the relationships between aggregation and vertical velocity. For example, several studies have shown that the vertical velocity profiles of tropical cyclones can be top-heavy (Nelson et al., 2019; Black et al., 1996), even though convection is highly aggregated. Similarly, vertical velocity profiles for squall lines and mesoscale convective systems can also be top-heavy, although there is wide variability (Garstang et al., 1994; Houze, 1989). Disentangling the links between aggregation and vertical velocity profiles thus remains an important priority for future research, and the isotopic composition of water vapor may be a valuable tool for such studies.

Our study raises some interesting questions on how convective aggregation may leave an isotopic signal in paleoclimate archives (Holloway et al., 2017). Several paleoclimate records have been interpreted as indicating the past frequency of organized convective systems (Medina-Elizalde & Rohling, 2012; Baldini et al., 2016; Maupin et al., 2021; Frappier et al., 2007) and in deep-time applications to snowball Earth (Abbot, 2014). The isotopic variations observed in the present study span about 25‰ between unaggregated and aggregated convection. While additional research is needed to exploit our results for paleoclimate applications, this range could plausibly be recorded in suitable proxy records. Furthermore, many paleoclimate studies interpret isotopic records in terms of the isotope amount effect, linking lower δ values to increased precipitation rates in the tropics (Lachniet, 2009), but our results here suggest that changes in convective aggregation could potentially confound such interpretations.

The results of this study may provide observational constraints for modeling studies, with relevance to the issues raised above. Our results from low I_{org} settings are consistent with the modeling study of Risi et al. (2021), who used large eddy simulations and a two-column model to show how water vapor δD values decrease with precipitation rate in unaggregated convection. They showed a close connection between the higher humidity in unaggregated convection and the mechanism for isotopically depleting the atmosphere. When the relative humidity is high in regions of ascent, there is less snow

sublimation and a smaller fraction of rain evaporation, with both effects leading to more depleted water vapor. In regions of large scale descent, entrainment of dry air into clouds reduces the vertical isotopic gradient and limits the depletion of tropospheric water vapor. Risi et al. (2021) did not compute D_{rl}, but the increasingly negative values of this parameter with precipitation rate for $I_{org} < 0.6$ would seem to support their conclusions.Risi et al. (2021) focused on unaggregated convection, but we found little change in D_{rl} with increasing precipitation rates for $I_{org} > 0.8$, which is consistent with their results for conditions of large-scale subsidence. Systematic, isotope-enabled modeling studies that sweep through a range of aggregation states could prove particularly fruitful for better understanding how convective aggregation impacts Earth's climate.

5 Conclusions

The goal of this study was to use remote sensing datasets of water vapor isotopic composition along with objective measures of convective aggregation to better understand the impact of convective aggregation on atmospheric water vapor. We found that unaggregated convection, with I_{org} below 0.6, is associated with a top-heavy vertical velocity profile and an anticorrelation between mixing ratio and water vapor δD with increasing convective intensity, consistent with partial hydrometeor evaporation. For I_{org} close to 0.5, water vapor δD values reach a minimum of around $-195‰$ at a mixing ratio of 8 g/kg and a precipitation rate of 20 mm/day. Highly aggregated convection (I_{org} above 0.8) is associated with a bottom-heavy vertical velocity profile and positive correlation between mixing ratio and δD, a result that is consistent with isotopic enrichment from detrainment of shallow convection near the observation level and with mixing of dry air from aloft. For I_{org} above 0.9, δD reaches a value of over $-170‰$ at a mixing ratio of 5 g/kg and a precipitation rate of 15 mm/day. Intermediate degrees of aggregation (I_{org} between 0.7 and 0.8) do not display significant variation in δD with mixing ratio or convective intensity, with δD remaining at around $-178‰$ regardless of precipitation rate. The results presented here provide a useful framework for better evaluating the links between convective aggregation and water vapor isotopic composition for a range of applications including the interpretation of paleoclimate archives and the evaluation of numerical simulations of convection.

6 Open Research

MUSICA IASI H2O,delD-pair data set: Diekmann, C. J., Schneider, M., and Ertl, B.: MUSICA IASI water isotopologue pair product (a posteriori processing version 2), Institute of Meteorology and Climate Research, Atmospheric Trace Gases and Remote Sensing (IMK-ASF), Karlsruhe Institute of Technology (KIT) [data set], https://doi.org/10.35097/415, 2021.

MUSICA IASI full retrieval product (includes among others vertically resolved H2O profiles): Schneider, M., Ertl, B., and Diekmann, C.: MUSICA IASI full retrieval product standard output (processing version 3.2.1), Karlsruhe Institute of Technology (KIT) [data set], https://doi.org/10.35097/408, 2021.

SAPHIR data (Brogniez et al., 2016) is available through the Aeris/ICARE ground segment of Megha-Tropiques (https://www.icare.univ-lille.fr/product-documentation/?product=SAPHIR-L2B-RH).

Acknowledgments

This work was supported by the LABEX-IPSL visitor program, the Franco-American Fulbright Foundation, and NSF AGS Grants 1738075 and 1158582 to JG; European Research Council (ERC) under the European Union's Horizon 2020 research program (Grant 694768) to SB and AG. Important developments of the MUSICA IASI processing were made during the project MUSICA (funded by the European Research Council under the European Community's Seventh Framework Programme (FP7/2007-2013), ERC grant agreement number 256961). The large-scale MUSICA IASI processing was supported by the Deutsche Forschungsgemeinschaft via the projects MOTIV (ID: 290612604) and TEDDY (ID: 416767181). The MUSICA IASI processing was performed on the supercomputer HoreKa funded by the Ministry of Science, Research and the Arts Baden-Württemberg and by the German Federal Ministry of Education and Research.

References

Abbot, D. S. (2014). Resolved Snowball Earth Clouds. *Journal of Climate*, *27*(12), 4391–4402. doi: 10.1175/jcli-d-13-00738.1

Bailey, A., Blossey, P. N., Noone, D., Nusbaumer, J., & Wood, R. (2017). Detecting shifts in tropical moisture imbalances with satellite-derived isotope ratios in

water vapor. *Journal of Geophysical Research: Atmospheres*, *122*(11), 5763–5779. doi: 10.1002/2016jd026222

Baldini, L. M., Baldini, J. U. L., McElwaine, J. N., Frappier, A. B., Asmerom, Y., Liu, K.-b., ... Breitenbach, S. F. M. (2016). Persistent northward North Atlantic tropical cyclone track migration over the past five centuries. *Scientific Reports*, *6*(1), 37522. doi: 10.1038/srep37522

Black, M. L., Burpee, R. W., & Jr., F. D. M. (1996). Vertical Motion Characteristics of Tropical Cyclones Determined with Airborne Doppler Radial Velocities. *Journal of the Atmospheric Sciences*, *53*(13), 1887–1909. doi: 10.1175/1520-0469(1996)053⟨1887:vmcotc⟩2.0.co;2

Bony, S., Semie, A., Kramer, R. J., Soden, B., Tompkins, A. M., & Emanuel, K. A. (2020). Observed Modulation of the Tropical Radiation Budget by Deep Convective Organization and Lower-Tropospheric Stability. *AGU Advances*, *1*(3). doi: 10.1029/2019av000155

Bretherton, C. S., Blossey, P. N., & Khairoutdinov, M. (2005). An Energy-Balance Analysis of Deep Convective Self-Aggregation above Uniform SST. *Journal of the Atmospheric Sciences*, *62*(12), 4273–4292. Retrieved from `http://ams.allenpress.com/perlserv/?request=get-abstract\&doi=10.1175\%2FJAS3614.1` doi: 10.1175/jas3614.1

Brogniez, H., Fallourd, R., Mallet, C., Sivira, R., & Dufour, C. (2016). Estimating Confidence Intervals around Relative Humidity Profiles from Satellite Observations: Application to the SAPHIR Sounder. *Journal of Atmospheric and Oceanic Technology*, *33*(5), 1005–1022. doi: 10.1175/jtech-d-15-0237.1

Chakraborty, S., Sinha, N., Chattopadhyay, R., Sengupta, S., Mohan, P. M., & Datye, A. (2016). Atmospheric controls on the precipitation isotopes over the Andaman Islands, Bay of Bengal. *Scientific Reports*, *6*(1), 19555. doi: 10.1038/srep19555

Craig, H. (1961). Isotopic Variations in Meteoric Waters. *Science*, *133*(346), 1702 1703. doi: 10.1126/science.133.3465.1702

Diekmann, C. J., Schneider, M., Ertl, B., Hase, F., García, O., Khosrawi, F., ... Braesicke, P. (2021). The global and multi-annual MUSICA IASI H2O, dD pair dataset. *Earth System Science Data*, *13*(11), 5273–5292. doi: 10.5194/essd-13-5273-2021

Diekmann, C. J., Schneider, M., Knippertz, P., Vries, A. J., Pfahl, S., Aemisegger, F., ... Braesicke, P. (2021). A Lagrangian Perspective on Stable Water Isotopes During the West African Monsoon. *Journal of Geophysical Research: Atmospheres*, *126*(19). doi: 10.1029/2021jd034895

Frappier, A. B., Sahagian, D., Carpenter, S. J., Gonzalez, L. A., & Frappier, B. R. (2007). Stalagmite stable isotope record of recent tropical cyclone events. *Geology*, *35*(2), 111–114. doi: 10.1130/g23145a.1

Galewsky, J. (2018a, 08). Relationships Between Inversion Strength, Lower-Tropospheric Moistening, and Low-Cloud Fraction in the Subtropical Southeast Pacific Derived From Stable Isotopologues of Water Vapor. *Geophysical Research Letters*, *45*(15), 7701 7710. doi: 10.1029/2018gl078953

Galewsky, J. (2018b). Using Stable Isotopes in Water Vapor to Diagnose Relationships Between Lower-Tropospheric Stability, Mixing, and Low-Cloud Cover Near the Island of Hawaii. *Geophysical Research Letters*, *45*(1), 297 305. doi: 10.1002/2017gl075770

Galewsky, J., & Hurley, J. V. (2010, 08). An advection-condensation model for subtropical water vapor isotopic ratios. *Journal of Geophysical Research: Atmospheres*, *115*(D16). doi: 10.1029/2009jd013651

Galewsky, J., Larsen, H. C. S., Field, R. D., Worden, J., Risi, C., & Schneider, M. (2016, 11). Stable isotopes in atmospheric water vapor and applications to the hydrologic cycle. *Reviews of Geophysics*, *54*(4). doi: 10.1002/2015rg000512

Garstang, M., Jr., H. L. M., Halverson, J., Greco, S., & Scala, J. (1994). Amazon Coastal Squall Lines. Part I: Structure and Kinematics. *Monthly Weather Review*, *122*(4), 608–622. doi: 10.1175/1520-0493(1994)122⟨0608:acslpi⟩2.0.co;2

Held, I. M., Hemler, R. S., & Ramaswamy, V. (1993). Radiative-Convective Equilibrium with Explicit Two-Dimensional Moist Convection. *Journal of the Atmospheric Sciences*, *50*(23), 3909–3927. doi: 10.1175/1520-0469(1993)050⟨3909:rcewet⟩2.0.co;2

Holloway, C. E., Wing, A. A., Bony, S., Muller, C., Masunaga, H., L'Ecuyer, T. S., ... Zuidema, P. (2017). Observing Convective Aggregation. *Surveys in Geophysics*, *38*(6), 1199 1236. doi: 10.1007/s10712-017-9419-1

Houze, R. A. (1989). Observed structure of mesoscale convective systems and implications for large-scale heating. *Quarterly Journal of the Royal Meteorological*

Society, *115*(487), 425–461. doi: 10.1002/qj.49711548702

Huffman, Stocker, E., Bolvin, D., Nelkin, E., & Tan, J. (2019). *GPM IMERG Final Precipitation L3 1 day 0.1 degree x 0.1 degree V06.* Retrieved from `https://doi.org/10.5067/GPM/IMERGDF/DAY/06`

Knapp, K. R., Ansari, S., Bain, C. L., Bourassa, M. A., Dickinson, M. J., Funk, C., ... Magnusdottir, G. (2011). Globally Gridded Satellite Observations for Climate Studies. *Bulletin of the American Meteorological Society*, *92*(7), 893–907. doi: 10.1175/2011bams3039.1

Kurita, N. (2013). Water isotopic variability in response to mesoscale convective system over the tropical ocean. *Journal Of Geophysical Research-Atmospheres*, *118*(18), 10376 10390. doi: 10.1002/jgrd.50754

Lachniet, M. S. (2009). Climatic and environmental controls on speleothem oxygen-isotope values. *Quaternary Science Reviews*, *28*(5-6), 412 432. doi: 10.1016/j.quascirev.2008.10.021

Lacour, J.-L., Risi, C., Worden, J., Clerbaux, C., & Coheur, P.-F. (2018). Importance of depth and intensity of convection on the isotopic composition of water vapor as seen from IASI and TES δD observations. *Earth and Planetary Science Letters*, *481*, 387–394. doi: 10.1016/j.epsl.2017.10.048

Lawrence, J. R., Gedzelman, S. D., Dexheimer, D., Cho, H. K., Carrie, G. D., Gasparini, R., ... Biggerstaff, M. I. (2004). Stable isotopic composition of water vapor in the tropics. *Journal Of Geophysical Research-Atmospheres*, *109*(D6). doi: 10.1029/2003jd004046

Lee, J.-E., & Fung, I. (2008, 01). "Amount effect" of water isotopes and quantitative analysis of post-condensation processes. *Hydrological Processes*, *22*(1), 1 8. doi: 10.1002/hyp.6637

Maupin, C. R., Roark, E. B., Thirumalai, K., Shen, C.-C., Schumacher, C., Kampen-Lewis, S. V., ... Partin, J. W. (2021). Abrupt Southern Great Plains thunderstorm shifts linked to glacial climate variability. *Nature Geoscience*, *14*(6), 396–401. doi: 10.1038/s41561-021-00729-w

Medina-Elizalde, M., & Rohling, E. J. (2012). Collapse of Classic Maya Civilization Related to Modest Reduction in Precipitation. *Science*, *335*(6071), 956–959. doi: 10.1126/science.1216629

Merlivat, L., & Jouzel, J. (1979). Global climatic interpretation of the deuterium-

oxygen 18 relationship for precipitation. *Journal of Geophysical Research: Oceans*, *84*(C8), 5029–5033. doi: 10.1029/jc084ic08p05029

Muller, C. J., & Held, I. M. (2012). Detailed Investigation of the Self-Aggregation of Convection in Cloud-Resolving Simulations. *Journal of the Atmospheric Sciences*, *69*(8), 2551–2565. doi: 10.1175/jas-d-11-0257.1

Nelson, T. C., Harrison, L., & Corbosiero, K. L. (2019). Examination of the Expendable Digital Dropsonde–Derived Vertical Velocities from the Tropical Cyclone Intensity (TCI) Experiment. *Monthly Weather Review*, *147*(7), 2367–2386. doi: 10.1175/mwr-d-18-0414.1

Noone, D. (2012). Pairing Measurements of the Water Vapor Isotope Ratio with Humidity to Deduce Atmospheric Moistening and Dehydration in the Tropical Midtroposphere. *Journal of Climate*, *25*(13), 4476–4494. doi: 10.1175/jcli-d-11-00582.1

Platnick, S., King, M. D., Ackerman, S. A., Menzel, W. P., Baum, B. A., Riedi, J. C., & Frey, R. A. (2003-02). The MODIS cloud products: Algorithms and examples from Terra. *Geoscience and Remote Sensing, IEEE Transactions on*, *41*(2), 459 473. doi: 10.1109/tgrs.2002.808301

Risi, C., Bony, S., Vimeux, F., Descroix, L., Ibrahim, B., Lebreton, E., ... Sultan, B. (2008). What controls the isotopic composition of the African monsoon precipitation? Insights from event-based precipitation collected during the 2006 AMMA field campaign. *Geophysical Research Letters*, *35*(24). doi: 10.1029/2008gl035920

Risi, C., Galewsky, J., Reverdin, G., & Brient, F. (2019). Controls on the water vapor isotopic composition near the surface of tropical oceans and role of boundary layer mixing processes. *Atmospheric Chemistry and Physics*, *19*(19), 12235–12260. doi: 10.5194/acp-19-12235-2019

Risi, C., Muller, C., & Blossey, P. (2021). Rain Evaporation, Snow Melt, and Entrainment at the Heart of Water Vapor Isotopic Variations in the Tropical Troposphere, According to Large-Eddy Simulations and a Two-Column Model. *Journal of Advances in Modeling Earth Systems*, *13*(4), e2020MS002381. doi: 10.1029/2020ms002381

Semie, A. G., & Bony, S. (2020). Relationship Between Precipitation Extremes and Convective Organization Inferred From Satellite Observations. *Geophysical Re-*

search Letters, *47*(9), e2019GL086927. doi: 10.1029/2019gl086927

Sivira, R. G., Brogniez, H., Mallet, C., & Oussar, Y. (2015). A layer-averaged relative humidity profile retrieval for microwave observations: design and results for the Megha-Tropiques payload. *Atmospheric Measurement Techniques*, *8*(3), 1055–1071. doi: 10.5194/amt-8-1055-2015

Team, G. S. (2022). *GPM DPR Spectral Latent Heating Profiles L2 1.5 hours 5 km V07.* Goddard Earth Sciences Data and Information Services Center. Retrieved from 10.5067/GPM/DPR/SLH/2H/07

Tobin, I., Roca, R., Tobin, I., Bony, S., & Roca, R. (2012, 06). Observational Evidence for Relationships between the Degree of Aggregation of Deep Convection, Water Vapor, Surface Fluxes, and Radiation. *dx.doi.org*, *25*(20), 6885 6904. doi: 10.1175/jcli-d-11-00258.1

Tompkins, A. M., & Semie, A. G. (2017, 06). Organization of tropical convection in low vertical wind shears: Role of updraft entrainment. *Journal of Advances in Modeling Earth Systems*, *9*(2), 1046 1068. doi: 10.1002/2016ms000802

Torri, G., Ma, D., & Kuang, Z. (2017). Stable water isotopes and large-scale vertical motions in the tropics. *Journal Of Geophysical Research-Atmospheres*, *122*(7), 3703 3717. doi: 10.1002/2016jd026154

Tremoy, G., Vimeux, F., Soumana, S., Souley, I., Risi, C., Favreau, G., & Oi, M. (2014). Clustering mesoscale convective systems with laser-based water vapor delta O-18 monitoring in Niamey (Niger). *Journal Of Geophysical Research-Atmospheres*, *119*(9), 5079 5103. doi: 10.1002/2013jd020968

Tsai, W.-M., & Mapes, B. E. (2022). Evidence of Aggregation Dependence of 5°-Scale Tropical Convective Evolution Using a Gross Moist Stability Framework. *Journal of the Atmospheric Sciences*, *79*(5), 1385–1404. doi: 10.1175/jas-d-21-0253.1

Wing, A. A., Emanuel, K., Holloway, C. E., & Muller, C. (2017). Convective Self-Aggregation in Numerical Simulations: A Review. *Surveys in Geophysics*, *38*(6), 1173–1197. doi: 10.1007/s10712-017-9408-4

Xu, T., Sun, X., Hong, H., Wang, X., Cui, M., Lei, G., ... Jiang, X. (2019). Stable isotope ratios of typhoon rains in Fuzhou, Southeast China, during 2013–2017. *Journal of Hydrology*, *570*, 445–453. doi: 10.1016/j.jhydrol.2019.01.017

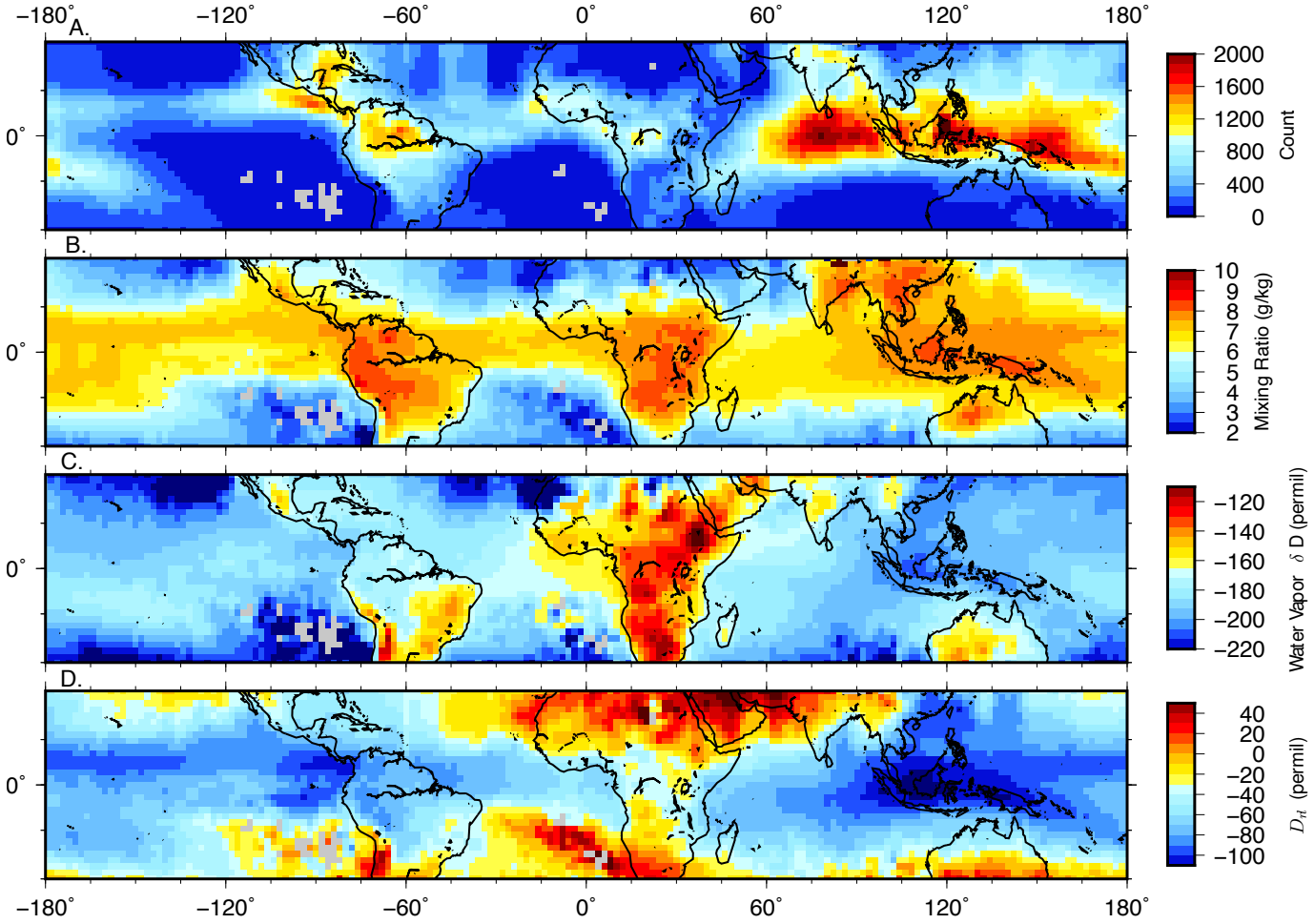

Figure 1. Maps for low I_{org} (between 0.5 and 0.65) from 2015-2020 for all precipitation rates. Data are averaged into 1x1 degree bins. (A) the count of data points in each bin; (B) mixing ratio from IASI; (C) water vapor dD; (D) deviation from Rayleigh distillation

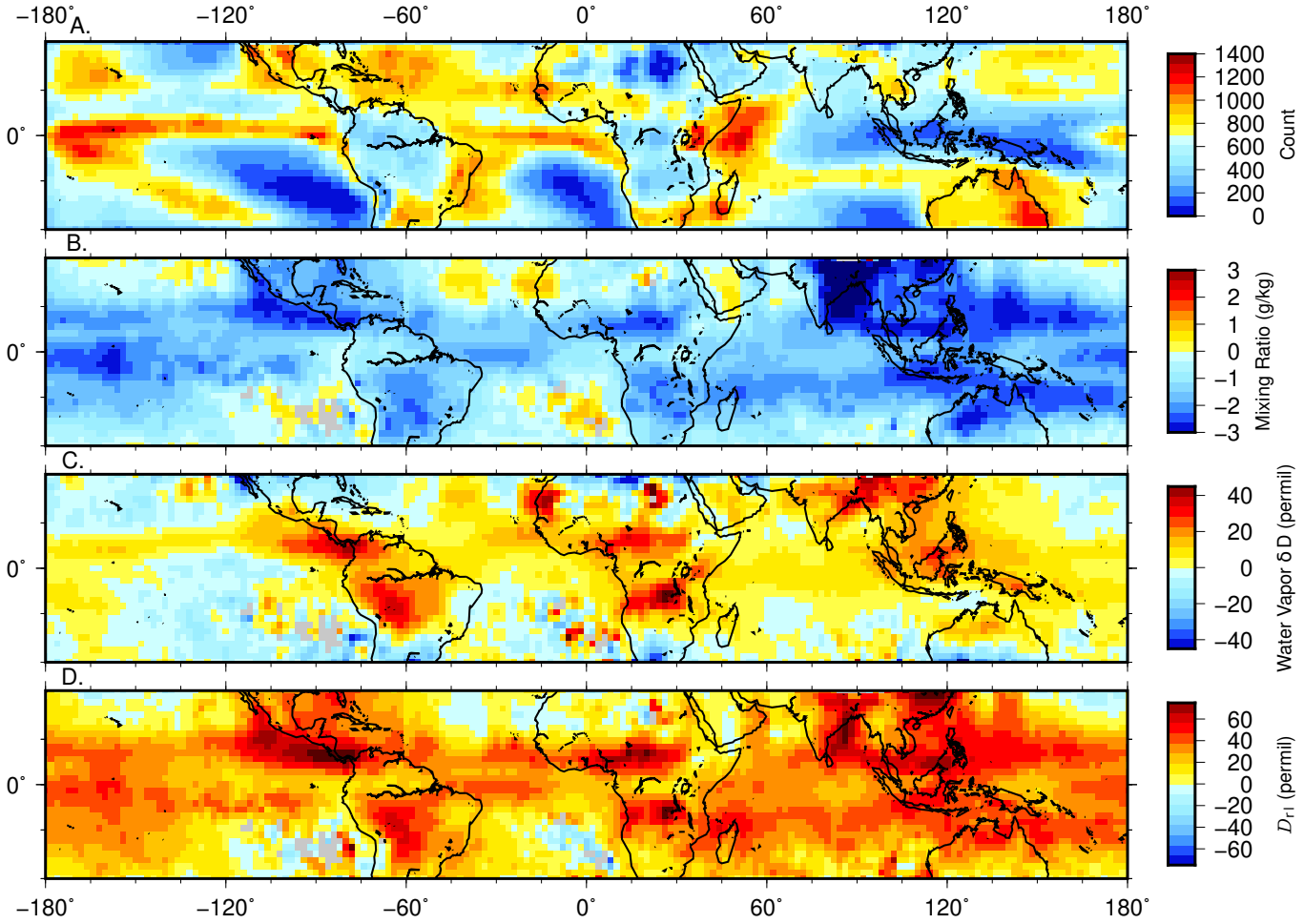

Figure 2. A: As in Figure 1 for high I_{org} (greater than 0.8). B-D: differences between high I_{org} and the low I_{org} fields in Figure 1.

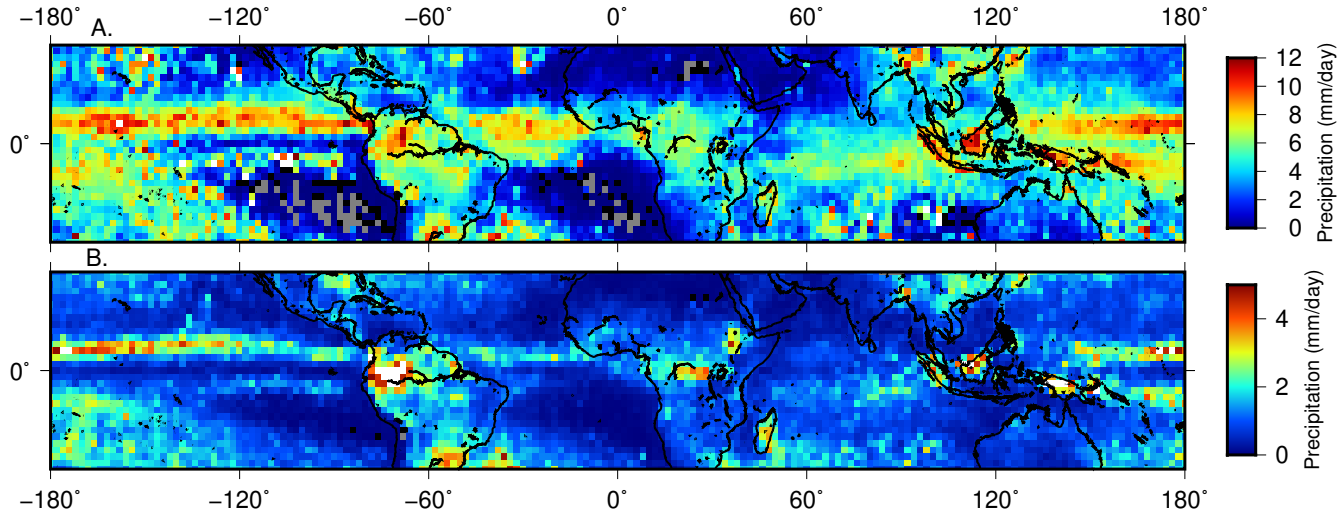

Figure 3. Average precipitation rate in mm/day for (A) I_{org} between 0.5 and 0.65 and (B) I_{org} above 0.8.

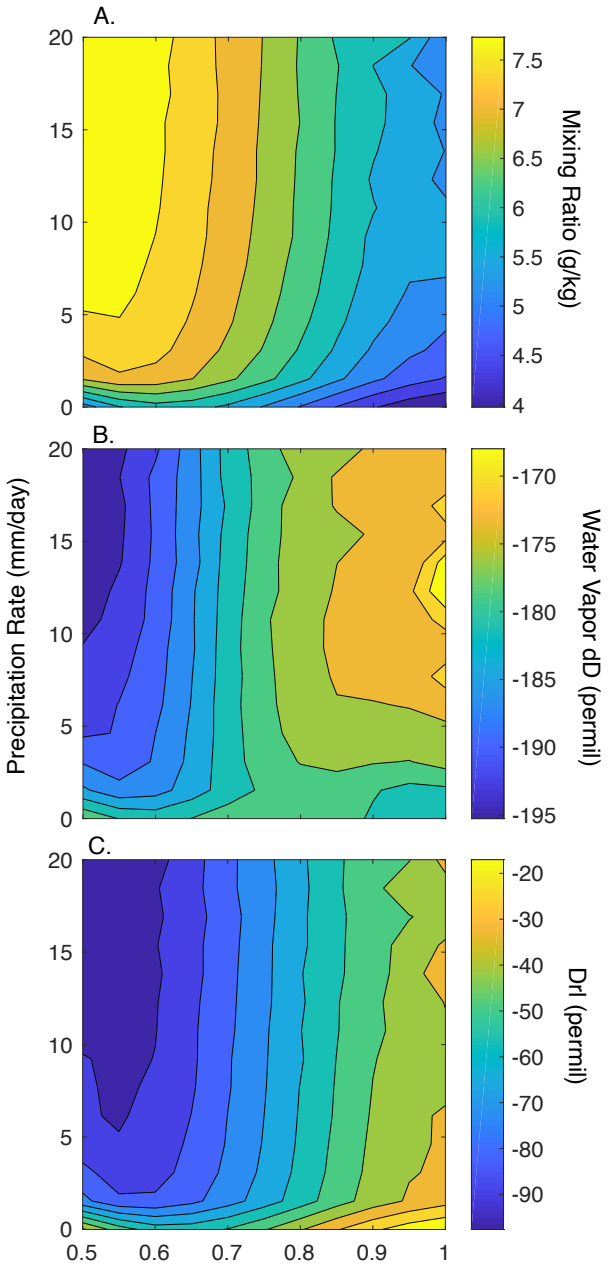

Figure 4. Bin-averaged (A) mixing ratio, (B) water vapor δD (permil), and (C) D_{RL} as a joint function of I_{org} and precipitation rate (mm/day).

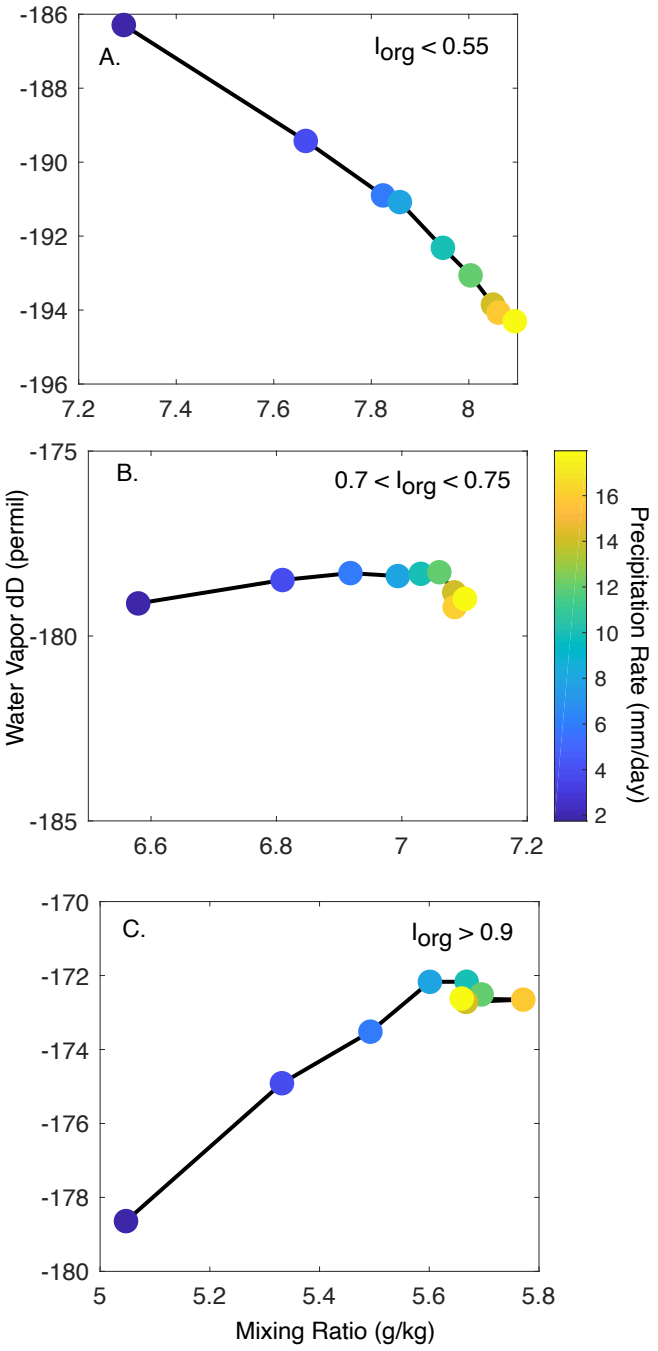

Figure 5. $q - \delta$ plots as a function of increasing precipitation rates for (A) $I_{org} < 0.55$; (B) $0.7 < I_{org} < 0.75$ and (C) $I_{org} > 0.9$. Colored dots indicate the precipitation rate. The y-axes in all panels span 10‰ to facilitate comparison.

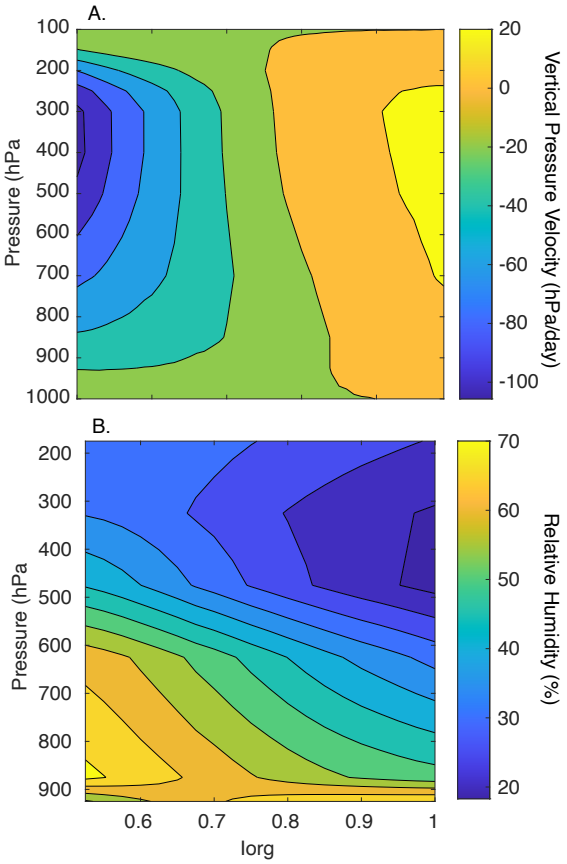

Figure 6. Average vertical profiles, sorted by I_{org}, of (A) ERA vertical pressure velocity (ω, hPa/day, (B) SAPHIR relative humidity

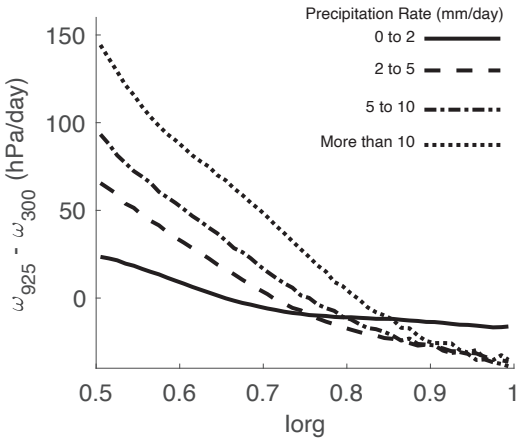

Figure 7. Difference between ω at 925 hPa and at 300 hPa, illustrating links between top-heaviness of convection as a function of I_{org} and precipitation rate.

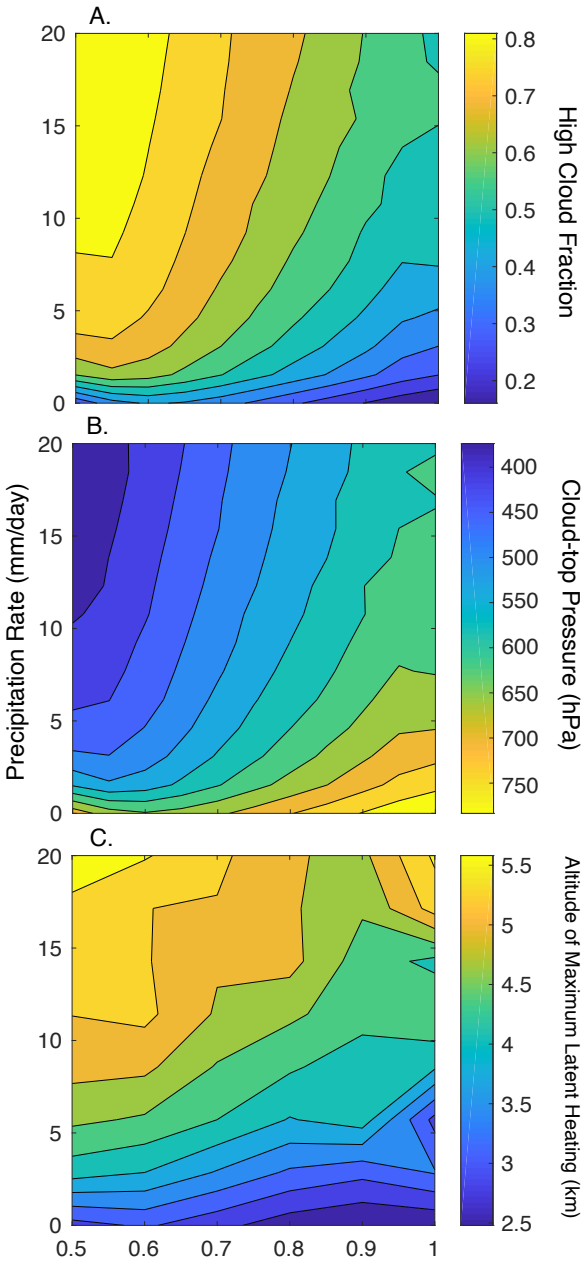

Figure 8. (a) High cloud fraction; (b) Cloud-top pressure; (c) Altitude of maximum latent heating, all plotted as bin-averaged values of I_{org} versus precipitation rate.

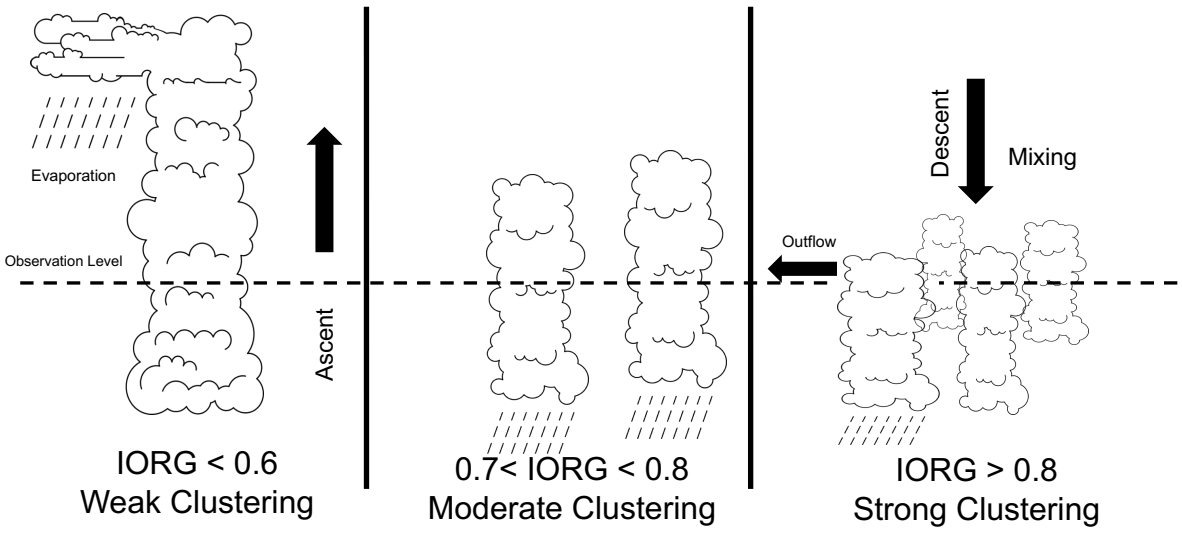

Figure 9. Cartoon summarizing the influence of different aggregation regimes on water vapor isotopic composition,